Acta Crystallographica Section B
Structural Science
ISSN 0108-7681

Order–disorder of oxygen anions and vacancies in solid solutions of La_2TiO_5 and $La_4Ga_2O_9$

Marta Kasunič,[a] Anton Meden,[a] Srečo D. Škapin,[b] Danilo Suvorov[b] and Amalija Golobič[a]*

[a]Faculty of Chemistry and Chemical Technology, University of Ljubljana, Aškerčeva 5, 1000 Ljubljana, Slovenia, and [b]Jožef Stefan Institute, Jamova 39, 1000 Ljubljana, Slovenia

Correspondence e-mail: amalija.golobic@fkkt.uni-lj.si

Received 13 February 2009
Accepted 17 July 2009

Successful Rietveld refinements of seven compounds with the formulae $La_2Ti_{(1-x)}Ga_xO_{(5-x/2)}$, where x = 0.00, 0.20, 0.50, 0.70, 0.90, 0.95 and 1.00, were performed in order to describe the solid solubility between orthorhombic (*Pnam*) La_2TiO_5 and monoclinic ($P2_1/c$) $La_4Ga_2O_9$. The relationship between the end-member structures, which are already known, is discussed; the space-group change is a consequence of ordering the oxygen vacancies that become more numerous as Ga is substituted for Ti. The structures of the solid solutions are also described. The lengths of cell edges obey Vegard's rule.

1. Introduction

Ceramics based on the La_2O_3–TiO_2 system show a good combination of dielectric properties which make them potential candidates for the manufacture of various components in electronic circuits (Marzullo & Bunting, 1958; Fuierer & Newnham, 1991; Takahashi *et al.*, 1991; Škapin *et al.*, 2000; Fasquelle *et al.*, 2005). On the other hand, $LaGaO_3$-based solid solutions posses high unipolar oxygen-ion conductivity and can therefore be used as oxygen sensors or oxygen-separation membranes and also in solid oxide fuel cells (Ishihara *et al.*, 1994; Zheng *et al.*, 2004; Martín-Sedeño *et al.*, 2004; Lerch *et al.*, 2001; Kajitani *et al.*, 2003).

Interesting properties of materials in both binary systems have led to the study of the La_2O_3–TiO_2–Ga_2O_3 ternary system. Until this work, structures of four ternary oxide compounds were known: $La_2Ti_{10.26}Ga_{9.63}O_{38}$ of davidite type (Meden *et al.*, 1999), $La_5GaTi_3O_{15}$ of perovskite type (Kuang *et al.*, 2006), and $La_3Ti_{1.11}Ga_{4.89}O_{14}$ (Takeda *et al.*, 1999) and $La_5Ti_4GaO_{17}$ (Titov *et al.*, 2007) of more complex structure types.

In the study of the subsolidus phase equilibria in the ternary La_2O_3–TiO_2–Ga_2O_3 system at 1573 K, a solid solubility in the entire compositional range between La_2TiO_5 and $La_4Ga_2O_9$ was identified. Seven solid solutions which form between the aforementioned end-members have the common formula $La_2Ti_{(1-x)}Ga_xO_{(5-x/2)}$ (x = 0.00, 0.20, 0.50, 0.70, 0.90, 0.95, 1.00). In order to explain the solid solubility, we had to find out:

(i) how their structures are related and what are the structures of the solid solutions, and

(ii) how the lengths of the cell edges depend on the composition of the solid solution.

To achieve this, Rietveld refinement with X-ray powder diffraction data was performed. Verification of the structures obtained was also achieved with bond-valence sum calculations.

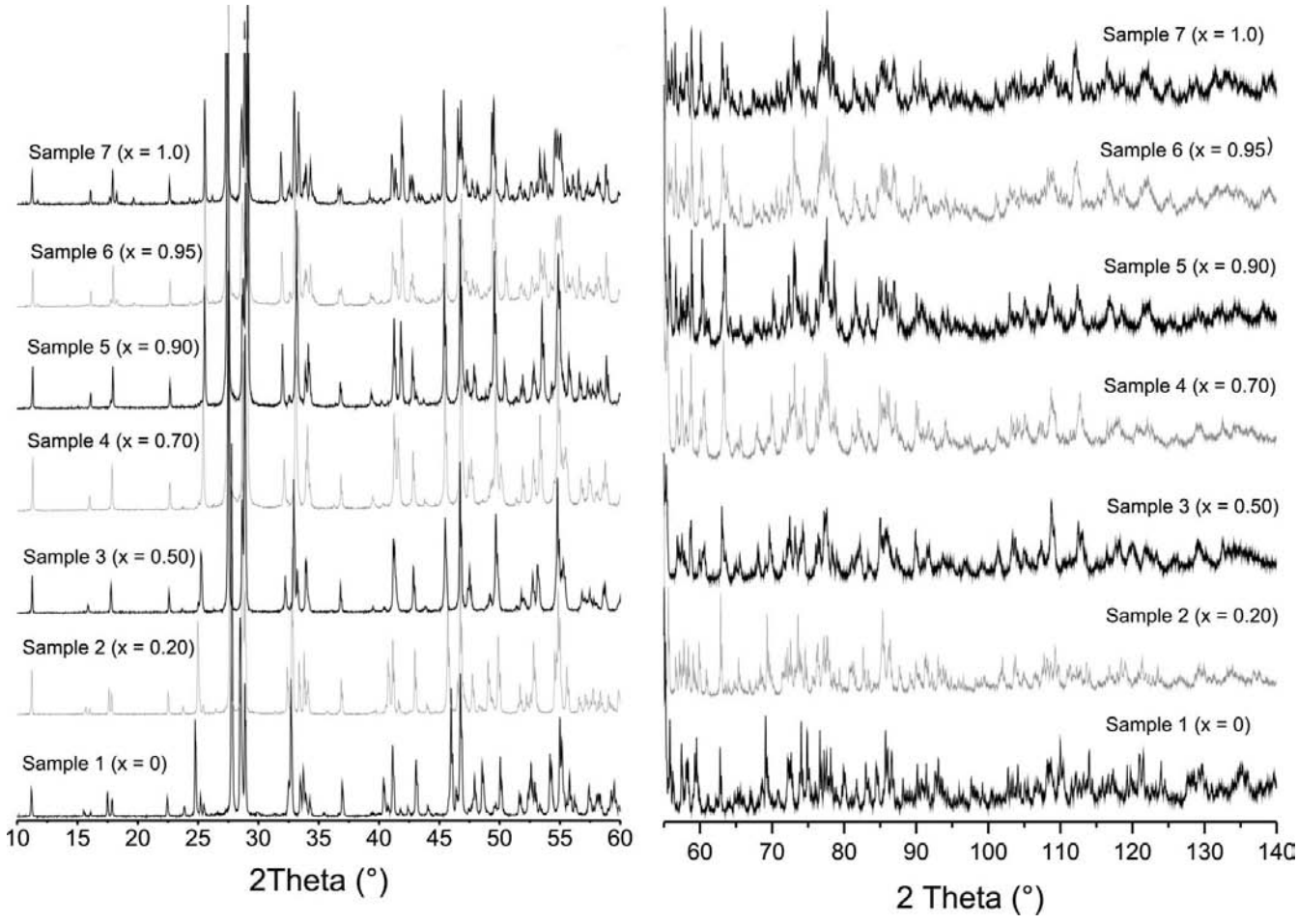

Figure 1
X-ray powder patterns of (1)–(7) in the region between 10 and 140° 2θ (intensity in arbitrary units). For the sake of a better representation of the patterns at high angles, the part from 55–140° 2θ was scaled by a factor of 2.

2. Experimental

The starting materials were La_2O_3 (Johnson Matthey, 99.9%), Ga_2O_3 (Aldrich Chem. Co., 99.99%) and TiO_2 (Ventron, 99.8%). The samples were prepared by solid-state reaction techniques according to the scheme: $La_2O_3 + (1-x)TiO_2 + (x/2)Ga_2O_3$ [or $(1-x)La_2TiO_5 + (x/2)La_4Ga_2O_9$] $\rightarrow La_2Ti_{(1-x)}Ga_xO_{(5-x/2)}$, where x = 0.00, 0.20, 0.50, 0.70, 0.90, 0.95 and 1.00 [samples (1)–(7)].

The weighed oxides were homogenized in an agate mortar with a pestle using acetone, pressed into pellets and calcined at 1573 K in air for approximately 60 h with intermittent fast cooling, crushing and remixing. The reaction was considered to be complete when X-ray patterns of successively fired samples showed no further change.

The X-ray diffraction patterns were collected on a Bruker AXS D4 Endeavor diffractometer with θ–2θ Bragg–Brentano geometry. The experimental profiles can be seen in Fig. 1. The crystal data, data collection and refinement data are presented in Table 1. The powder patterns of (1)–(5) are similar. The patterns of (1)–(5) were indexed with an orthorhombic unit cell which was very similar to that of La_2TiO_5. On the other hand, in the powder patterns of (6) and (7) splitting of strong reflections and the appearance of some new peaks were observed. These were indexed with a monoclinic unit cell, similar to that of $La_4Ga_2O_9$, a cell which is twice as large as the orthorhombic cell of La_2TiO_5. Fig. 2 shows the enlarged regions of powder patterns of (5), (6) and (7) where new and split reflections appear. The match between calculated and observed profiles for all samples in the range between 10–60° 2θ is presented in Fig. 3. The Rietveld plots for the full 2θ range are available as supplementary material[1] (Fig. 3*a*).

As starting models, unit-cell parameters and coordinates of La_2TiO_5 (Guillen & Bertaut, 1966) for (1)–(5) and those of $La_4Ga_2O_9$ (Martín-Sedeño *et al.*, 2004) for (6) and (7) were used. In order to treat both end-members in the same manner as the intermediate solid solutions, their structural parameters were also refined. Rietveld refinements were performed using the *TOPAS Academic*, Version 4.1, program suite (Coelho, 2007). At first, only four background parameters, a specimen displacement and a scale factor were refined. In the following least-square cycles, the refinement of unit-cell parameters and a parameter for crystallite size were turned on. Afterwards, the atomic positions were refined – the coordinates of gallium

[1] Supplementary data for this paper are available from the IUCr electronic archives (Reference: KD5032). Services for accessing these data are described at the back of the journal.

Table 1
Crystal data, data collection and refinement data.

	(1)	(2)	(3)	(4)
Crystal data				
Chemical formula	La_2TiO_5	$La_2Ti_{0.8}Ga_{0.2}O_{4.9}$	$La_2Ti_{0.5}Ga_{0.5}O_{4.75}$	$La_2Ti_{0.3}Ga_{0.7}O_{4.65}$
M_r	405.69	408.47	412.62	415.39
Crystal system, space group	Orthorhombic, *Pnam*	Orthorhombic, *Pnam*	Orthorhombic, *Pnam*	Orthorhombic, *Pnam*
Temperature (K)	293	293	293	293
a, *b*, *c* (Å)	11.00713 (11), 11.40018 (11), 3.94377 (4)	11.04452 (11), 11.28420 (11), 3.96519 (4)	11.09937 (19), 11.14255 (17), 3.98321 (5)	11.13674 (16), 11.06383 (15), 3.98631 (5)
V (Å^3)	494.88 (1)	494.18 (1)	492.62 (1)	491.17 (1)
Z	4	4	4	4
Radiation type	Cu $K\alpha$	Cu $K\alpha$	Cu $K\alpha$	Cu $K\alpha$
Wavelength of incident radiation (Å)	1.5418	1.5418	1.5418	1.5418
μ (mm^{-1})	143.889	142.659	140.949	139.924
Specimen form, colour	Irregular, pale yellow powder	Irregular, pale yellow powder	Irregular, pale yellow powder	Irregular, pale yellow powder
Data collection				
Diffractometer	Bruker AXS D4 Endeavor	Bruker AXS D4 Endeavor	Bruker AXS D4 Endeavor	Bruker AXS D4 Endeavor
Specimen mounting	Flat plate	Flat plate	Flat plate	Flat plate
Scan method	Step	Step	Step	Step
Data-collection mode	Reflection	Reflection	Reflection	Reflection
2θ values (°)	$2\theta_{min}$ = 10, $2\theta_{max}$ = 140, $2\theta_{step}$ = 0.02	$2\theta_{min}$ = 10, $2\theta_{max}$ = 140, $2\theta_{step}$ = 0.02	$2\theta_{min}$ = 10, $2\theta_{max}$ = 140, $2\theta_{step}$ = 0.02	$2\theta_{min}$ = 10, $2\theta_{max}$ = 140, $2\theta_{step}$ = 0.02
Refinement				
R_p, R_{wp}, R_{exp}, χ^2	0.090, 0.120, 0.068, 3.10	0.093, 0.122, 0.071, 2.96	0.088, 0.115, 0.070, 2.72	0.082, 0.105, 0.0563, 3.46
Excluded regions	None	None	None	None
No. of data points	6501	6501	6501	6501
No. of parameters	33	33	33	33
No. of restraints	0	0	0	0

	(5)	(6)	(7)
Crystal data			
Chemical formula	$La_2Ti_{0.1}Ga_{0.9}O_{4.55}$	$La_4Ti_{0.10}Ga_{1.90}O_{9.05}$	$La_4Ga_2O_9$
M_r	418.16	837.68	839.08
Crystal system, space group	Orthorhombic, *Pnam*	Monoclinic, $P2_1/c$	Monoclinic, $P2_1/c$
Temperature (K)	293	293	293
a, *b*, *c* (Å)	11.17394 (16), 10.99713 (14), 3.98992 (5)	7.98014 (9), 11.19613 (14), 11.64676 (14)	7.98082 (8), 11.20250 (11), 11.62961 (11)
β (°)	490.29 (1)	109.5310 (9)	109.4874 (7)
V (Å^3)	490.29 (1)	980.72 (2)	980.19 (2)
Z	4	4	4
Radiation type	Cu $K\alpha$	Cu $K\alpha$	Cu $K\alpha$
Wavelength of incident radiation (Å)	1.5418	1.5418	1.5418
μ (mm^{-1})	138.729	138.348	138.061
Specimen shape, colour	Irregular, pale yellow powder	Irregular, pale yellow powder	Irregular, pale yellow powder
Data collection			
Diffractometer	Bruker AXS D4 Endeavor	Bruker AXS D4 Endeavor	Bruker AXS D4 Endeavor
Specimen mounting	Flat	Flat	Flat
Scan method	Step	Step	Step
Data-collection mode	Reflection	Reflection	Reflection
2θ values (°)	$2\theta_{min}$ = 10, $2\theta_{max}$ = 140, $2\theta_{step}$ = 0.02	$2\theta_{min}$ = 10, $2\theta_{max}$ = 140, $2\theta_{step}$ = 0.02	$2\theta_{min}$ = 10, $2\theta_{max}$ = 140, $2\theta_{step}$ = 0.02
Refinement			
R_p, R_{wp}, R_{exp}, χ^2	0.084, 0.109, 0.056, 3.72	0.067, 0.090, 0.055, 2.66	0.062, 0.086, 0.060, 2.07
Excluded region(s)	None	None	None
No. of data points	6501	6501	6501
No. of parameters	33	63	63
No. of restraints	0	0	0

Computer programs used: *TOPAS-Academic*, Version 4.1 (Coelho, 2007), *ATOMS* (Dowty, 2005), *CRYSCON* (Dowty, 2006).

were constrained to be equal to those of titanium. In the next steps, one parameter for strain, three additional background parameters and atomic isotropic displacement parameters were gradually refined. The latter were constrained to be equal for similar types of atoms. According to EDS (energy-dispersive X-ray spectroscopy) analysis, which was in agreement with the synthesis ratio, the population parameters of the metal ions were constrained to $La_2Ti_{(1-x)}Ga_xO_{(5-x/2)}$.

Table 2
Labeling of atoms due to conversion into monoclinic cell.

La_2TiO_5	La1	La2	O1	O2	O3	O4	O5
$La_4Ga_2O_9$	La1*a*, La1*b*	La2*a*, La2*b*	O1*a*, O1*b*	O2*a*, O2*b*	O3*a*, vacancy/O3*v*	O4*a*, O4*b*	O5*a*, O5*b*

There was a question about the population parameters of O-atom sites in the solid solutions. The exchange of titanium ions with the gallium ones leads to a change of charge that is balanced by the formation of oxygen vacancies. In (2)–(5) these are disordered. Their ordering in (6)–(7) lowers the symmetry from orthorhombic to monoclinic and doubles the unit-cell volume. Two fully occupied atomic positions in the monoclinic unit cell of $La_4Ga_2O_9$ correspond to each of the atoms O1, O2, O4 and O5 in the orthorhombic unit cell. This does not hold true for an orthorhombic O3 atom since only one of its two corresponding monoclinic positions is occupied and the second is empty (the detailed description of atom labels can be seen in Table 2). Thus, oxygen vacancies in $La_4Ga_2O_9$ are ordered on this site. Since the oxygen vacancies are ordered on half of the O3 sites in monoclinic (6) and (7), it was assumed that the oxygen vacancies in orthorhombic (2)–(5) are located at O3 sites only and that their positions on these sites is random.

On the other hand, the *Pnam* symmetry is also retained when the vacancies are randomly positioned over all five oxygen sites. In this model, the refinement of population parameters of O atoms resulted in unacceptable values since some population parameters exceeded 1. The result of trial refinements of oxygen occupancies was very similar whether or not a constraint on the total oxygen occupancy was applied.

There is nothing surprising in that as the scattering power of oxygen is much smaller than those of the metal ions included. Interestingly, the refinement of population parameters of O1, O2, O4 and O5 for (3), (4) and (5) resulted in values larger than the starting average $(1 - x/10)$ and only the population parameter of O3 decreased. This was not only true for (2) where the refinement of the population parameters of O atoms indicated a lower occupancy for the O2 atom, probably due to the smaller amount of oxygen vacancies. When complete structure refinements of (3)–(5) was performed using fixed population parameters of (*a*) $1 - x/10$ for all five O atoms, and (*b*) 1 for O1, O2, O4 and O5 atoms, and $1 - x/2$ for O3 atom, the refinement R_{wp} values were slightly smaller for the second case, with the exception of (2) where the R_{wp} values were practically the same for both calculations. Therefore, a decision to perform the final refinements with fixed population parameters equal to 1 for four O atoms and the fixed population parameter $1 - x/2$ for O3 atom was made. This approach was confirmed by the final structures; at the end, it was also possible to explain the change in cell edges with the composition of the solid solutions. Note that in all of the described refinements the total oxygen occupancy was constrained appropriately according to the expected formula.

In order to estimate the stability of structures of both end-members, *i.e.* orthorhombic La_2TiO_5 and monoclinic $La_4Ga_2O_9$, single-point quantum chemical calculations using the Cambridge Serial Total Energy Package (CASTEP; Clark *et al.*, 2005) were performed. CASTEP is an *ab initio* density-functional theory plane-wave pseudopotential code that is intended for the simulation of periodic systems. The calculations were carried out using full crystallographic symmetry; the unit-cell parameters and the positions of the atoms were fixed. The atomic charges and bond-overlap populations were determined by the default Mulliken population analysis.

3. Results and discussion

3.1. Structural relationship between end-members: La_2TiO_5 and $La_4Ga_2O_9$

Fig. 4 shows a projection of La_2TiO_5 structure along its *a* axis. Titanium ions are positioned on a mirror plane and coordinated by five oxygen anions in the shape of a distorted trigonal bipyramid. Through O3 and its mirror image, these bipyramids are connected into infinite chains along the *c* axis of the orthorhombic unit cell. Fig. 5 represents a projection of the $La_4Ga_2O_9$ structure along its *b* axis which corresponds to the *a* axis of the orthorhombic unit cell. The structures are

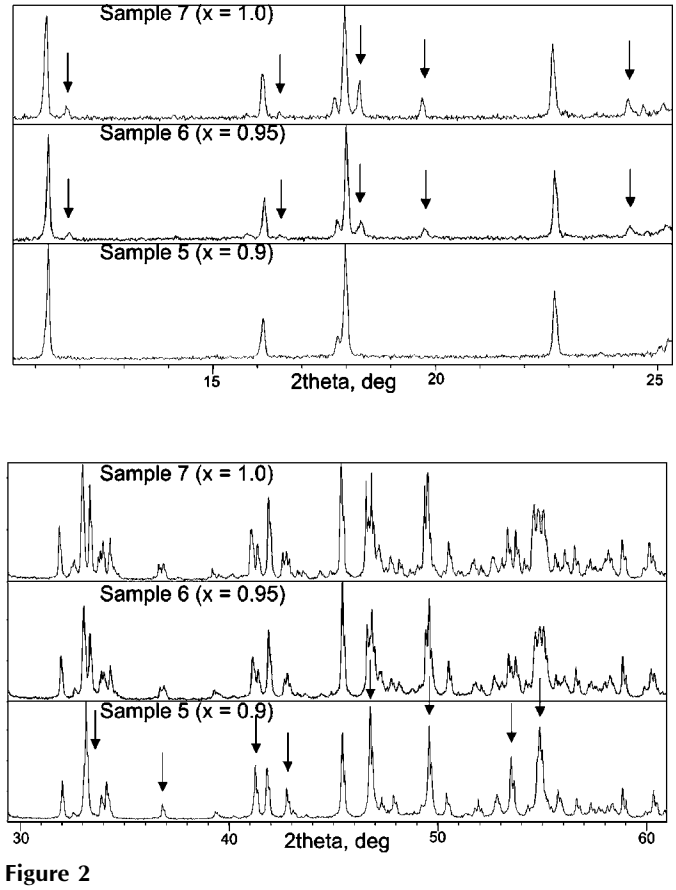

Figure 2
The enlarged regions of powder patterns of samples (5), (6) and (7) showing the appearance of new reflections and the splitting of some reflections in (6) and (7) owing to the lowering of symmetry according to oxygen-vacancy ordering (intensity in arbitrary units).

similar except that along the *a* monoclinic axis in $La_4Ga_2O_9$ one half of the sites corresponding to O3 in La_2TiO_5 are empty and consequently, there are only pairs of distorted tetrahedra instead of infinite chains of TiO_5 bipyramids. In other words, if every second O3 site in the structure of La_2TiO_5 had been unoccupied, the resulting structural motif would have been very similar to that of $La_4Ga_2O_9$. Besides that, in the structure of La_2TiO_5 it is possible to choose a doubled unit cell (outlined in Fig. 4) which is very similar to the monoclinic unit cell of $La_4Ga_2O_9$. The matrix for the transformation from the orthorhombic unit cell to the corresponding doubled monoclinic one is $(00\bar{2}, \bar{1}00, 011)$ and for the inverse operation $(0\bar{1}0, \frac{1}{2}01, \bar{\frac{1}{2}}00)$. All transformations were performed using the *CRYSCON* software (Dowty, 2006). Figs. 6 and 7 present a view of the structure along the chains of bipyramids or pairs of tetrahedra: along the *c* axis for La_2TiO_5 and along the *a* axis for $La_4Ga_2O_9$. Again, a significant similarity between the structures of the two end-members can be seen.

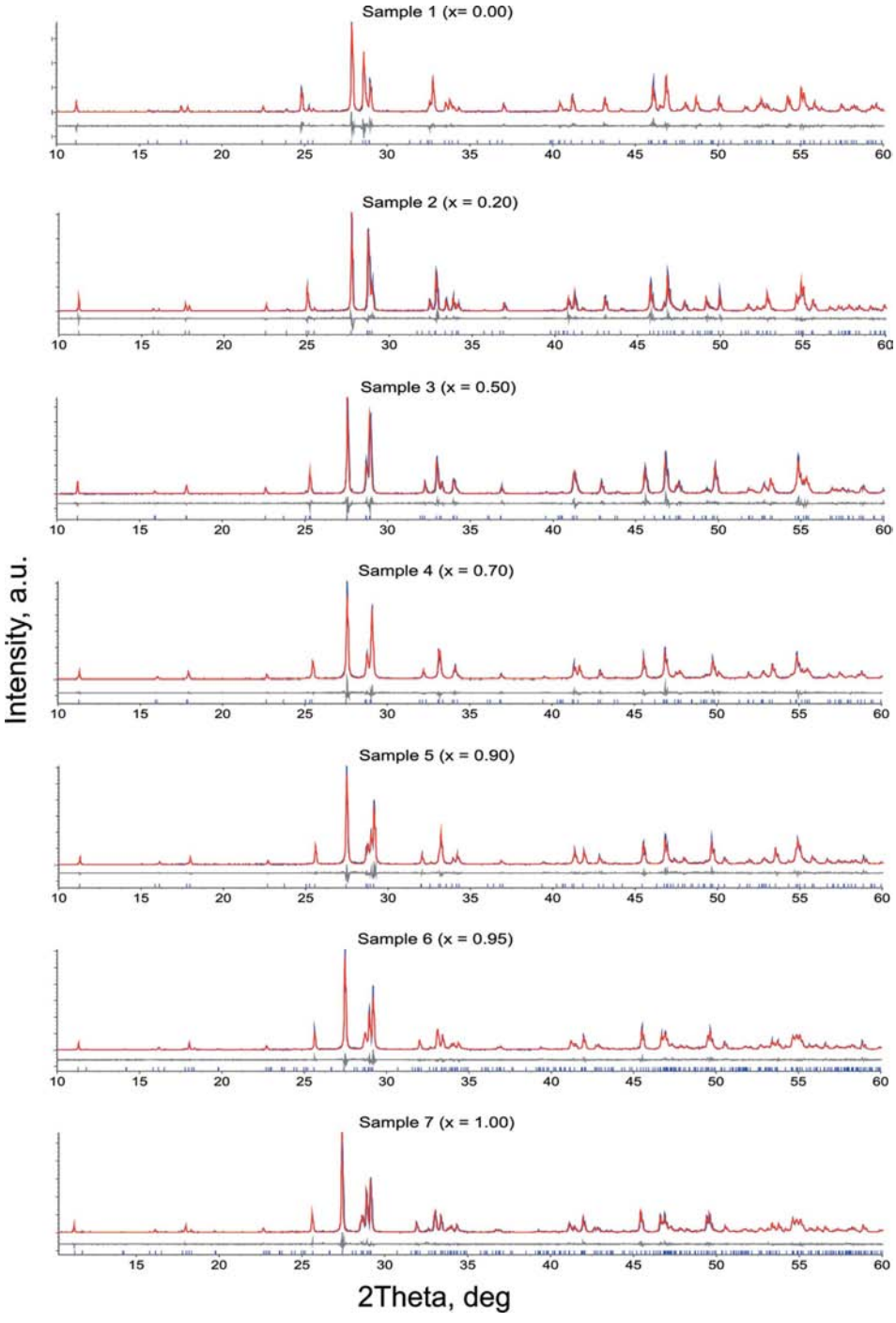

Figure 3
Experimental (blue), calculated (red) and difference profiles of (1)–(7) in the range between 10 and 60° 2θ. Lower vertical bars represent reflection positions. This figure is in colour in the electronic version of this paper.

3.2. Structures of solid solutions

In the solid solutions, gallium cations randomly replace titanium. The charge is balanced by the oxygen vacancies which in (2)–(5) are randomly distributed on the O3 sites. At the beginning, it could not be excluded that the oxygen vacancies are randomly positioned over all oxygen sites. In both cases, the orthorhombic *Pnam* space-group symmetry is retained and only the cell edges are slightly different. As already mentioned, in the powder patterns of (6) and (7) some reflections are split and some new reflections appear due to the ordering of the oxygen vacancies and these can only be indexed with a doubled monoclinic unit cell. The ordering of the oxygen vacancies on one half of the O3 sites doubles the orthorhombic *c* axis and causes accommodation of the other atoms, which results in the lowering of the symmetry from orthorhombic *Pnam* to monoclinic $P2_1/c$. In that way, the chains of bipyramids are broken and gallium ions are moved closer to the occupied O3 site along the monoclinic *a* axis. In the structure of La_2TiO_5 and in the other orthorhombic solid solutions the bond between Ti/Ga and O3 [from 2.033 (3) to 2.070 (6) Å] is longer than the remaining Ti/Ga—O bonds [from 1.680 (16) to 1.910 (13) Å], which is not the case in both monoclinic structures where all the Ti/Ga—O bond lengths are between 1.76 (3) and 2.00 (3) Å. This is also connected with the fact that in (2)–(5) Ti/Ga and O3 lie on the neighbouring mirror planes and their

Table 3
Selected distances between oxygen and metal ions (Å; labels correspond to the orthorhombic O atoms).

Sample	x	La—O	Ti/Ga—O3	Ti/Ga—O (O2, O4, O5)
La_2TiO_5†	0	2.341 (11)–2.569 (11)	2.027 (3)	1.744 (14)–1.922 (16)
1	0	2.418 (13)–2.593 (13)	2.034 (3)	1.788 (13)–1.908 (13)
2	0.2	2.408 (14)–2.628 (15)	2.041 (4)	1.733 (15)–1.889 (14)
3	0.5	2.381 (17)–2.999 (17)	2.037 (5)	1.705 (17)–1.865 (16)
4	0.7	2.378 (16)–2.908 (16)	2.065 (6)	1.772 (15)–1.851 (15)
5	0.9	2.375 (15)–2.893 (14)	2.065 (7)	1.797 (15)–1.838 (15)
6	0.95	2.33 (3)–2.99 (3)	1.72 (3) 2.04 (3)	1.75 (3)–1.90 (3)
7	1.0	2.33 (3)–2.92 (2)	1.73 (3) 1.99 (3)	1.76 (2)–1.89 (3)
$La_4Ga_2O_9$‡	1.0	2.365 (6)–2.946 (7)	1.858 (8) 1.873 (8)	1.814 (6)–1.857 (6)

† Guillen & Bertaut (1966). ‡ Martín-Sedeño *et al.* (2004).

bond distance is symmetry constrained. No further conclusions on the basis of La—O and Ti/Ga—O distances presented in Table 3 can be drawn. Although the bond lengths are comparable to the corresponding ones in the literature (Guillen & Bertaut, 1966; Martín-Sedeño *et al.*, 2004), the values do not show any trend of regular enlargement or reduction owing to the change in composition. Namely, because of the low scattering power of O atoms compared with those of metal ions (Ti^{4+}, Ga^{3+} and La^{3+}) the Rietveld refinement of X-ray powder patterns generally cannot determine the positions of O atoms very accurately.

The graph in Fig. 8 presents the dependence of the unit-cell parameters and the volume on the composition. The orthorhombic lattice parameter b nearly decreases linearly, while a and c increase with an increasing amount of substitution obeying Vegard's rule. The difference in the effective ionic radii (0.51 Å for five-coordinated Ti^{4+} and 0.47 Å for four-coordinated Ga^{3+}; Shannon, 1976) should contribute to the small contraction of the unit cell in all three directions with the enlargement of x. On the contrary, the introduction of oxygen vacancies on the O3 sites should have an opposite effect. Namely, the O3 anion in La_2TiO_5 is surrounded with three La^{3+} ions (marked with + and # in Figs. 6 and 7) lying in the same mirror plane as O3 (best seen in Fig. 4) and in the direction of the c axis with two Ti^{4+} ions lying on both parallel neighbouring mirror planes. The oxygen vacancy on this site should cause some repulsion among all the surrounding positive ions and consequently contribute to the expansion of the unit cell in all three directions. This is supported by the distances among cations around the O3 site which on average increase with an increasing x value, which can be seen in Table 4. For (6) and (7) the upper value in Table 4 corresponds to the ions around the vacancy and the lower value to those around the occupied site. The expansion of a and c orthorhombic parameters indicates that the cation repulsion around the vacant O3 site predominates over the contraction because of the smaller cations, while the contraction of the orthorhombic b axis indicates a significant influence of the following structure feature. In La_2TiO_5, Ti^{4+} and two La^{3+} ions (marked with * in Figs. 6 and 7) lie on the same mirror plane. During the exchange of Ti^{4+} with Ga^{3+} ions, which still lie on the same mirror plane in the orthorhombic solid solutions, the contraction of the b edge can be explained with the reduction of positive charge which consequently reduces the repulsion between cations and shortens the distances between them. In

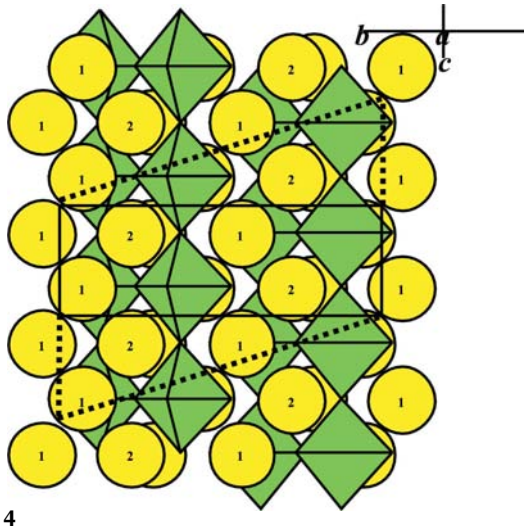

Figure 4
Projection of the structure of La_2TiO_5 along its a axis. The conventional (orthorhombic) unit cell is drawn with a solid line and the unconventional doubled monoclinic unit cell with a dotted line. O atoms not bound to Ti are omitted for clarity. Circles represent La cations (numericals used instead of full atom names, *e.g.* 1 for La1 *etc.*). Trigonal bipyramids represent coordinated Ti cations.

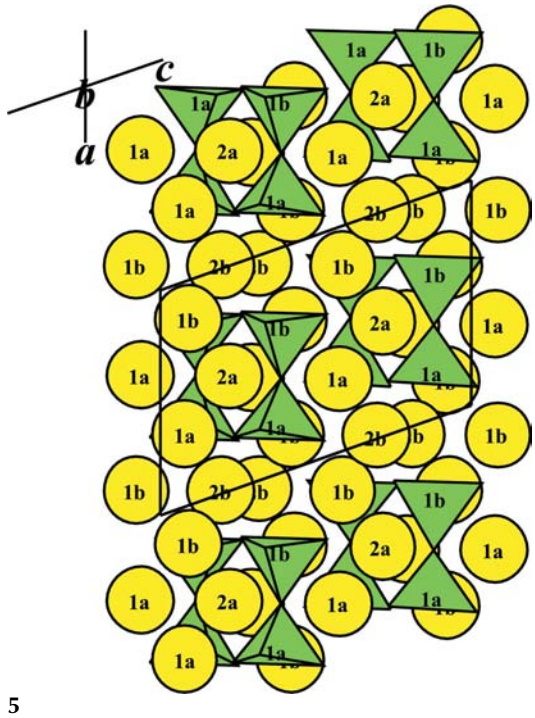

Figure 5
Projection of the structure of $La_4Ga_2O_9$ along its b axis (corresponding to the a axis of the orthorhombic unit cell). O atoms not bound to Ga are omitted for clarity. Circles represent La cations (numericals used instead of full atom names, *e.g.* 1a for La1a *etc.*) and pairs of tetrahedra represent coordinated Ga cations.

Table 4
Distances between cations around the O3 site (Å; labels correspond to Figs. 6 and 7).

Sample	x	La2+···La2#	Sym. code	La2+···La1+	Sym. code	La1+···La2#	Sym. code	Ti/Ga···Ti/Ga	Sym. code
La_2TiO_5†	0	5.540 (7)	i, ii	3.960 (8)	i, iii	5.948 (7)	iii, ii	3.9300 (1)	viii, i
1	0	5.565 (2)	i, ii	3.991 (2)	i, iii	5.957 (2)	iii, ii	3.9438 (1)	viii, i
2	0.2	5.588 (2)	i, ii	4.012 (2)	i, iii	5.977 (2)	iii, ii	3.9652 (1)	viii, i
3	0.5	5.625 (2)	i, ii	4.064 (2)	i, iii	6.027 (2)	iii, ii	3.9832 (1)	viii, i
4	0.7	5.657 (2)	i, ii	4.118 (2)	i, iii	6.040 (2)	iii, ii	3.9863 (1)	viii, i
5	0.9	5.683 (2)	i, ii	4.145 (2)	i, iii	6.067 (2)	iii, ii	3.9899 (1)	viii, i
6	0.95	5.741 (4)	iv, v	4.313 (4)	iv, vii	5.992 (5)	vii, v	4.430 (10)	ix, x
		5.660 (4)	iv, vi	3.985 (4)	iv, iv	6.166 (4)	iv, vi	3.554 (10)	ix, ix
7	1.0	5.752 (3)	iv, v	4.343 (3)	iv, vii	5.992 (4)	vii, v	4.483 (8)	ix, x
		5.663 (3)	iv, vi	3.967 (3)	iv, iv	6.156 (4)	iv, vi	3.502 (8)	ix, ix
$La_4Ga_2O_9$‡	1.0	5.749 (3)	iv, v	4.336 (4)	iv, vii	5.994 (4)	vii, v	4.487 (6)	ix, x
		5.667 (3)	iv, vi	3.967 (4)	iv, iv	6.161 (4)	iv, vi	3.496 (6)	ix, ix

Symmetry codes: (i) $-x+1, -y+1, z-\frac{1}{2}$; (ii) $-x+\frac{3}{2}, y+\frac{1}{2}, z-\frac{1}{2}$; (iii) $x+\frac{1}{2}, -y+\frac{1}{2}, -z+\frac{1}{2}$; (iv) x, y, z; (v) $-x, y+\frac{1}{2}, -z+\frac{3}{2}$; (vi) $-x+1, y+\frac{1}{2}, -z+\frac{3}{2}$; (vii) $x-1, y, z$; (viii) $-x+1, -y+1, z+\frac{1}{2}$; (ix) $x+1, -y+\frac{3}{2}, z+\frac{1}{2}$; (x) $x, -y+\frac{3}{2}, z+\frac{1}{2}$. † Guillen & Bertaut (1966). ‡ Martín-Sedeño *et al.* (2004).

the monoclinic phases [(6) and (7)], the introduction of gallium ions instead of titanium ones and oxygen vacancies on half of the O3 sites causes a movement of Ga^{3+} toward the occupied O3 site (*i.e.* movement away from the mirror plane which does not exist any more). This enables the reduction of an average distance between La^{3+} ions (marked with *) in the *b* orthorhombic direction (distances are given in Table 5), causing the reduction of the *b* cell edge with an increasing *x* value. When considering the trends in the variation of distances between metal ions with the degree of replacement of Ti^{4+} with Ga^{3+}, it can be concluded that also in the orthorhombic solid solutions oxygen vacancies are positioned on only the O3 sites. A plot of the unit-cell volume *versus* composition in Fig. 8 shows that the volume decreases with the enlargement of *x*, from which it can be concluded that the overall effect of substitution of Ti^{4+} with Ga^{3+} and the creation of oxygen vacancies is a reduction of the unit-cell volume.

In order to confirm the above-described pattern of Ti/Ga substitution and the arrangement of oxygen vacancies, bond-valence calculations according to Brown & Altermatt (1985) were performed for the structures of (1)–(7). The sums of bond valences for metal ions are presented in Table 6. The obtained atomic valences of La, Ti and Ga are close to the nominal values 3, 4 and 3, confirming the reliability of the results of the structure analysis. Smaller deviations from expectations for (6) might be an indication that this compound is less stable than the others. The trial refinement in the orthorhombic unit cell and *Pnam* symmetry for (6) resulted in a significantly worse agreement between calculated and observed diffraction patterns. Additionally, the calculated sums of bond valences of the obtained structure deviate from the expected nominal cation valences much more.

In similar solid solutions with Ga/Ge substitution (Martín-Sedeño *et al.*, 2004) with the formulae $La_2Ge_{0.1}Ga_{0.9}O_{4.55}$,

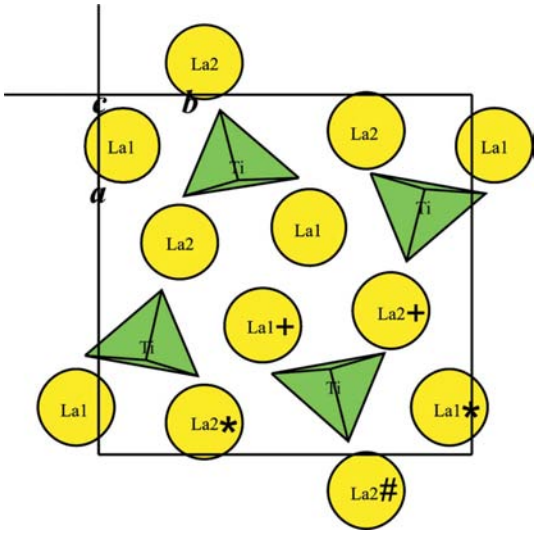

Figure 6
Projection of the structure of La_2TiO_5 along its *c* axis. Labels *, + and # correspond to Tables 4 and 5. O atoms not bound to Ti are omitted for clarity.

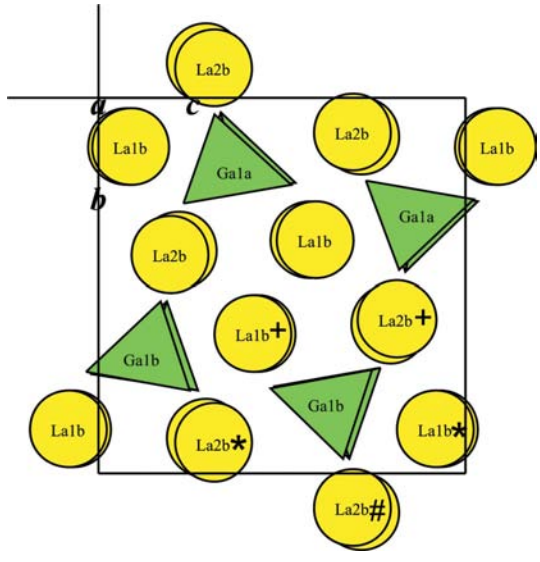

Figure 7
Projection of the structure of $La_4Ga_2O_9$ along its *a* axis (corresponding to the *c* axis of the orthorhombic unit cell). Labels *, + and # correspond to Tables 4 and 5. O atoms not bound to Ga are omitted for clarity.

Table 5
Distances between La1* and La2* (labels correspond to Figs. 6 and 7).

Sample	x	La1*···La2*	Symmetry codes
La_2TiO_5†	0	7.448 (8)	i, ii
1	0	7.448 (2)	i, ii
2	0.2	7.309 (2)	i, ii
3	0.5	7.109 (2)	i, ii
4	0.7	6.975 (2)	i, ii
5	0.9	6.878 (2)	i, ii
6	0.95	6.797 (4), 6.911 (4)	iii, iv
7	1.0	6.786 (3), 6.886 (3)	iii, iv
$La_4Ga_2O_9$‡	1.0	6.800 (4), 6.876 (4)	iii, iv

Symmetry codes: (i) $-x+1, -y+1, z+\frac{1}{2}$; (ii) $x+\frac{1}{2}, -y+\frac{1}{2}, -z+\frac{3}{2}$; (iii) $x, -y+\frac{3}{2}, z+\frac{1}{2}$; (iv) $x, -y+\frac{3}{2}, z-\frac{1}{2}$. † Guillen & Bertaut (1966). ‡ Martín-Sedeño *et al.* (2004).

Table 6
Bond-valence sums for metal ions (to 3.000 Å from each cation).

	La1	La2	Ti	Ga
La_2TiO_5†	2.973	3.269	4.040	–
Sample1	3.004	3.085	3.936	–
Sample2	2.881	3.016	4.022	3.197
Sample3	2.737	3.045	4.007	3.185
Sample4	2.914	2.902	3.696	2.937
Sample5	2.803	2.943	3.585	2.849

	La1*a*	La1*b*	La2*a*	La2*b*	Ti1*a*	Ti1*b*	Ga1*a*	Ga1*b*
Sample 6	2.660	3.071	2.814	3.021	4.233	3.405	3.364	2.706
Sample 7	2.991	2.635	2.967	2.778	–	–	3.175	3.182
$La_4Ga_2O_9$†	2.810	2.888	2.935	2.914	–	–	2.999	2.955

† Guillen & Bertaut (1966). † Martín-Sedeño *et al.* (2004).

$La_2Ge_{0.2}Ga_{0.8}O_{4.6}$ and $La_2Ge_{0.3}Ga_{0.7}O_{4.65}$ [which would correspond to $La_2Ge_{(1-x)}Ga_xO_{(5-x/2)}$, where x = 0.9, 0.8 and 0.7], the structures of all three compounds were found to be monoclinic with the symmetry $P2_1/c$ and isostructural to $La_4Ga_2O_9$. On the contrary, only the compound with a composition very close to $La_4Ga_2O_9$, *i.e.* $La_2Ti_{0.05}Ga_{0.95}O_{4.525}$ (6), is found to be monoclinic while all the other compounds [(2)–(5)] with x = 0.2, 0.5, 0.7 and 0.9 are orthorhombic. In order to reject the possibility of the analogous lower (monoclinic) symmetry in (2)–(5), where indexing and systematic absences show an otherwise smaller unit cell with higher (orthorhombic) symmetry, the final orthorhombic structures of (2)–(5) were converted to the monoclinic cell. Three cases of oxygen-vacancy ordering were studied: with O3*a* fully and O3*v* only partially occupied, with equal occupation of O3*a* and O3*v*, and for the case where the occupancies of both sites were refined (for labeling see Table 2). The total oxygen occupancy was always constrained to reflect the known oxygen content. After the Rietveld refinement procedure (with practically the same or worse R_{wp} values than for the orthorhombic ones), still a reasonable geometry was obtained and bond-valence sums were calculated. These are collected in Table 7 of the supplementary material. For all the three cases for (2)–(5), the atomic valences obtained for La, Ti and Ga deviate from the expected nominal values 3, 4 and 3. This additionally proves the accuracy of the structure analysis including the arrangement of oxygen vacancies in (2)–(5).

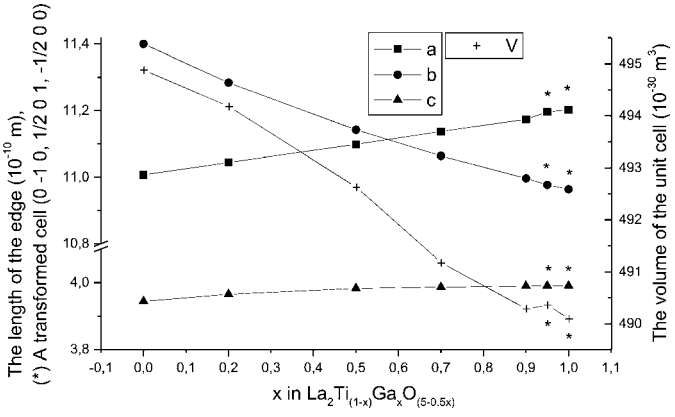

Figure 8
The dependence of the unit-cell parameters (left) and the unit-cell volume on the composition. Monoclinic cell parameters (marked with *) were transformed to the orthorhombic cell with the transformation matrix $(0\bar{1}0, \frac{1}{2}01, \frac{1}{2}00)$.

A crucial difference in the two series [$La_2Ge_{(1-x)}Ga_xO_{(5-x/2)}$ and $La_2Ti_{(1-x)}Ga_xO_{(5-x/2)}$] is a tendency of the germanium ions to have fourfold coordination (structures with fivefold coordination of germanium ions are not known), while for titanium ions fivefold coordination (and also sixfold) is possible and usual. This can also be observed in the structures of La_2GeO_5 (Berastegui *et al.*, 2002) with fourfold coordination and La_2TiO_5 with fivefold coordination of Ge or Ti, respectively. The structures are completely different and only for the La_2TiO_5 structure can a similarity with $La_4Ga_2O_9$ be seen, as described in this paper. This is probably the reason for the existence of a solid solubility between La_2TiO_5 and $La_4Ga_2O_9$ in the entire compositional range, while for $La_2Ge_{(1-x)}Ga_xO_{(5-x/2)}$ only solid solutions with x larger than 0.7 are known.

An additional confirmation of the appearance of orthorhombic structures in the majority of the compositions in the studied $La_2Ti_{(1-x)}Ga_xO_{(5-x/2)}$ series can also be presented by the quantum calculations for the end-members, from which the orthorhombic end-member seems to be more stable than the monoclinic one. Namely, Mulliken charges for La_2TiO_5 are 1.49, 1.52 and 0.82 for La and Ti atoms, and −0.82, −0.77, −0.73, −0.77 and −0.73 for O atoms. On the other hand, charges for the $La_4Ga_2O_9$ are 1.50, 1.51, 1.62, 1.52, 0.77 and 0.81 for La and Ga atoms, and −0.86, −0.86, −0.87, −0.86, −0.88, −0.87, −0.86, −0.83 and −0.82 for O atoms.

4. Conclusions

The structural relationships between both structures of the end-members (La_2TiO_5 and $La_4Ga_2O_9$) and the structures of their solid solutions were elucidated. In the solid solutions, Ti^{4+} ions are randomly replaced by Ga^{3+} ions and the charge is balanced by oxygen vacancies which seem to be randomly positioned on O3 sites in the orthorhombic structures. On the other hand, the splitting of some reflections and the appear-

ance of some new peaks in the diffraction patterns of $La_2Ti_{0.05}Ga_{0.95}O_{4.525}$ and $La_4Ga_2O_9$ [(6) and (7)] were explained as a consequence of the oxygen-vacancy ordering. This causes the lowering of the symmetry (monoclinic $P2_1/c$ rather than orthorhombic *Pnam*) and doubling of the unit cell. Additionally, the solid solubility can be proved by application of Vegard's rule to this system. With the replacement of titanium by gallium (*i.e.* with increasing x value) the structure contracts along the orthorhombic b axis and expands along the remaining two edges.

Financial support of the Ministry of Higher Education, Science and Technology of the Republic of Slovenia is gratefully acknowledged (grants P2-0091, P1-0175 and MR-29397). The authors also wish to thank Dr James Kaduk for quantum chemical calculations and his help with their interpretation.

References

Berastegui, P., Hull, S., Garcia Garcia, F. J. & Grins, J. (2002). *J. Solid State Chem.* **168**, 294–305.
Brown, I. D. & Altermatt, D. (1985). *Acta Cryst.* B**41**, 244–247.
Clark, S. J., Segall, M. D., Pickard, C. J., Hasnip, P. J., Probert, M. J., Refson, K. & Payne, M. C. (2005). *Z. Kristallogr.* **220**, 567–570.
Coelho, A. A. (2007). *TOPAS-Academic*, Version 4.1. Coelho Software, Brisbane, Australia.
Dowty, E. (2005). *ATOMS*, Version 6.2. Shape Software, Kingsport, USA.
Dowty, E. (2006). *CRYSCON*, Version 1.2.1. Shape Software, Kingsport, USA.
Fasquelle, D., Carru, J. C., Le Gendre, L., Le Paven, C., Pinel, J., Cheviré, F., Tessier, F. & Marchand, R. (2005). *J. Eur. Ceram. Soc.* **25**, 2085–2088.
Fuierer, P. A. & Newnham, N. E. (1991). *J. Am. Ceram. Soc.* **74**, 2876–2881.
Guillen, M. & Bertaut, E. F. (1966). *C. R. Hebd. Seances Acad. Sci. B*, **262**, 962–965.
Ishihara, T., Matsuda, H. & Takita, Y. (1994). *J. Am. Chem. Soc.* **116**, 3801–3803.
Kajitani, M., Matsuda, M., Hoshikawa, A., Oikawa, K. I., Torii, S., Kamiyama, T., Izumi, F. & Miyake, M. (2003). *Chem. Mater.* **15**, 3468–3473.
Kuang, X., Allix, M. M. B., Claridge, J. B., Niu, H. J., Rosseinsky, M. J., Ibberson, R. M. & Iddles, D. M. (2006). *J. Mater. Chem.* **16**, 1038–1045.
Lerch, M., Boysen, H. & Hansen, T. (2001). *J. Phys. Chem. Solids*, **62**, 445–455.
Martín-Sedeño, M. C., Losilla, E. R., León-Reina, L., Bruque, S., Marrero-López, D., Núñez, P. & Aranda, M. A. G. (2004). *Chem. Mater.* **16**, 4960–4968.
Marzullo, S. & Bunting, E. N. (1958). *J. Am. Ceram. Soc.* **41**, 40–41.
Meden, A., Kolar, D. & Skapin, S. (1999). *Powder Diffr.* **14**, 36–41.
Shannon, R. D. (1976). *Acta Cryst.* A**32**, 751–767.
Škapin, S. D., Kolar, D. & Suvorov, D. (2000). *J. Eur. Ceram. Soc.* **20**, 1179–1185.
Takahashi, J., Kageyama, K. & Hayashi, T. (1991). *Jpn. J. Appl. Phys.* **30**, 2354–2358.
Takeda, H., Kato, T., Chani, V. I., Shimamura, K. & Fukuda, T. (1999). *J. Alloys Compd.* **290**, 244–249.
Titov, Y. A., Belyavina, N. M., Markiv, V. Ya., Slobodyanik, M. S., Chumak, V. V. & Yashchuk, V. P. (2007). *J. Alloys Compd.* **430**, 81–84.
Zheng, F., Bordia, R. K. & Pederson, L. R. (2004). *Mater. Res. Bull.* **39**, 141–155.